

Robust shape optimization using artificial neural networks based surrogate modeling for an aircraft wing

Moussaoui Z.¹, Karafi Y.¹, Abou El Majd B.^{1,2}

¹*LMSA Laboratory, Faculty of Science, Mohammed V University in Rabat, Morocco*

²*University of Lille, 59655 Villeneuve-d'Ascq, France*

(Received 31 May 2023; Revised 16 February 2024; Accepted 17 February 2024)

Aerodynamic shape optimization is a very active area of research that faces the challenges of highly demanding Computational Fluid Dynamics (CFD) problems, optimization with Partial Differential Equations (PDEs) as constraints, and the appropriate treatment of uncertainties. This includes the development of robust design methodologies that are computationally efficient while maintaining the desired level of accuracy in the optimization process. This paper addresses aerodynamic shape optimization problems involving uncertain operating conditions. After a review of possible approaches to account for uncertainties, an Artificial Neural Network (ANN) model is used to approximate the aerodynamic coefficients when the operating conditions vary. Robust optimization problem-solving approaches based on deterministic measurements are used, inspired by the work of Deb [Deb K., Gupta H. Introducing robustness in multi-objective optimization. KanGAL Report 2004–2016, Kanpur Genetic Algorithms Laboratory, Indian Institute of Technology, Kanpur, India (2004)]. The first procedure is a direct extension of a technique used for single-objective optimization. The second is a more practical approach allowing a user to define the desired degree of robustness in a problem. These approaches have been tested and validated in the case of the optimization of an aircraft wing profile in the transonic regime considering two uncertain variables: the Mach number and the angle of incidence.

Keywords: *shape optimization; aerodynamic analysis; free-form deformation; surrogate model; uncertainty modeling; artificial neural networks.*

2010 MSC: 65Kxx

DOI: 10.23939/mmc2024.01.139

1. Introduction

In recent years, the continuous progress of Computational Fluid Dynamics (CFD) has paved the way for optimization, mainly of shape and design by numerical simulation of incompressible aerodynamics and its coupling with other disciplines. Optimal design in aerodynamics is a field at the interface of several classical disciplines where many technical components must be assembled. As a result, shape optimization raises many challenging topics in numerical analysis, concurrent engineering, and software development. These include the development of robust optimizers that take uncertainty into account in the optimization process.

Deterministic shape optimization techniques or deterministic computational fluid dynamics (CFD) simulations have been widely used in engineering to improve product quality. However, many uncertain factors arise in the practical design and application. Deterministic optimization has not considered the influence of uncertainties. Its optimal form can be susceptible to uncertainties, leading to poor off-design performance and even failure to meet the design requirements. Instead of deterministic shape optimization, a new shape optimization called Robust Design Optimization (RDO) has been proposed in recent years. A shape optimized by a deterministic shape optimization approach may not achieve the expected performance for industrial problems due to these errors and uncertainties. In the context of Robust Aerodynamic Design Optimization (RADO), robust design implies that the performance of the final configuration is insensitive to uncertainties in the operating conditions and the geometry. The objective of RADO is to optimize the quality of a product and, at the same time, to reduce the impact of uncertainties on product performance. Compared to traditional deterministic optimization.

An essential element of RADO is Uncertainty quantifications (UQ), which can significantly increase the computational expense of the design process compared to the computational effort of deterministic optimization. The optimization of aerodynamic shapes is a very active research area that has to face the challenges posed by very demanding computational fluid dynamics (CFD) problems by optimization with partial differential equations (PDEs) as constraints and by the appropriate treatment of uncertainties. Therefore it is essential to develop an advanced approach and implement robust design methodologies that are computationally efficient while maintaining the desired level of accuracy in the optimization process.

A generalized RADO process has been developed to efficiently solve problems related to RADO. This process involves constructing a mathematical expression and an optimization model based on a given problem description. The flowchart in Figure 1 illustrates four important steps of the general RADO process.

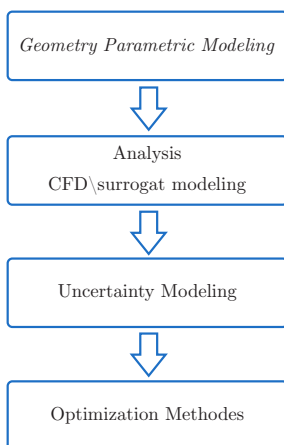


Fig. 1. RADO process.

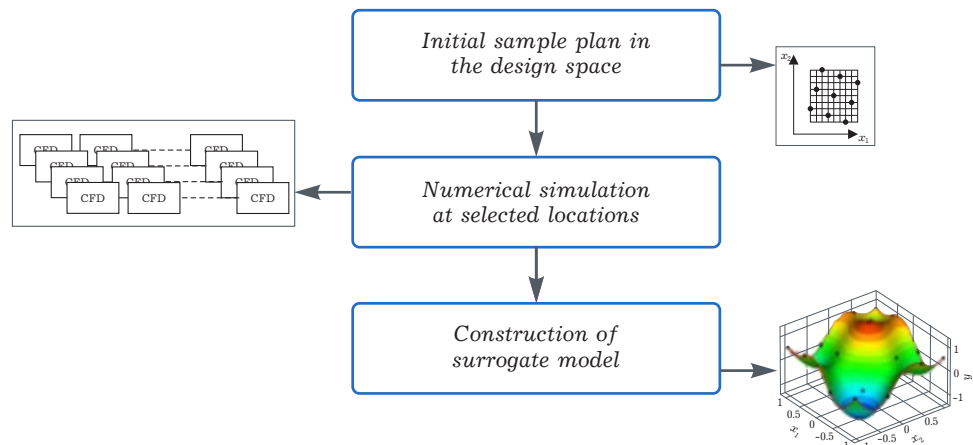


Fig. 2. Surrogate model framework.

The first step is to choose an a priori geometric representation of the shapes and, consequently, to search for a robust shape for a given problem. With parametric geometry modeling, the form of the geometry is represented and deformed by design variables based on a specific geometry parameterization method. The most common geometric parameterization methods include spline methods. D. I. Papadimitriou and C. Papadimitriou [1] used Bezier curves to parameterize a 2D aerodynamic profile. J. Nagawkar et al. [2], X. Du, and L. Leifsson [3] have used B-spline for 2D aerodynamic shapes in RADO. In works [4–7], the airfoil geometry is represented using Kulfan’s Class and Shape Function Transformation (CST) method. While optimization establishes performance measures from computational fluid dynamics (CFD), deformational methods are the most straightforward for defining the body surface. A commonly used method for aerodynamic optimization is the free-form deformation (FFD) approach, which is helpful if the geometry manipulations are particularly complex. It has more advantages in terms of deformability for general three-dimensional configurations. The mentioned studies [8, 9] successfully achieved efficient optimization of aerodynamic profiles by employing FFD parameterization.

In an attempt to develop an automated shape optimization strategy, as mentioned above, flow simulation is performed by computational fluid dynamics (CFD) to evaluate the aerodynamic response of the system, which is then coupled with optimization algorithms to enable the search for the optimal geometry. The aerodynamic performance is predicted by a CFD simulation which includes the generation or deformation of the mesh and the solution of the equations governing viscous or inviscid flows, such as the Navier–Stokes (N-S) or Euler equations, etc. Solving the N-S equations requires a fine grid and a higher computational cost. The works [10, 11] used the decoupling solver TAU provided by the DLR¹ which allows for an approximation of the aerodynamic coefficients and their gradients by the

¹German Aerospace Center, (DLR)

adjoint approach. Due to the computational intensity of CFD simulation, the surrogate model technique (also called meta-model) has been widely used to approximate the N-S equation solver to provide efficient evaluations. The surrogate model involves establishing a mathematical approximation model, which uses previously obtained sample data to predict objective function values at untested points, Figure 2 shows the framework of the surrogate model. Works [5–7] have used the Kriging model to predict aerodynamic parameters. Papers [3,12] used the Polynomial Chaos Expansion (PCE) model. J. Nagawkar and L. Leifsson [2] proposed the Polynomial Chaos Cokriging (PC-Cokriging) model. They compared this meta-model to Kriging, Polynomial Chaos Expansion (PCE), Polynomial Chaos Kriging (PC-Kriging), and Cokriging in the case of robust airfoil design optimization. According to the work of [13], the Bayesian Neural Network (BNN) model was employed to forecast aerodynamic parameters. Jun Tao et al., [4] used a PCA-DBN substitution model based on Principal Component Analysis (PCA) and Deep Belief Network (DBN). The parameterization method applies the PCA technique to the geometric parameters. The DBN model is established to predict the aerodynamic parameters, with the reduced design variables as input and the aerodynamic parameters as output. PCA-DBN is applied to robust aerodynamic design optimizations of a natural laminar flow (NLF) airfoil and a transonic wing.

An essential aspect of RADO is UQ. Effective UQ methods can improve the computational efficiency of robust aerodynamic optimization. Two types of input uncertainty must be considered in robust aerodynamic design studies: uncertainties in operating conditions (e.g., Reynolds or Mach number, angle of attack, etc.) and geometric uncertainties (e.g., manufacturing uncertainties, etc.). Probability distribution functions (PDFs) are often used to quantify uncertainties in simulations, and probability calculus is applied to propagate uncertainties. Optimal design under uncertainty is usually formulated as a problem of minimizing a weighted average of the mean value and standard deviation of a performance function subject to reliability constraints expressed in terms of the probability of unacceptable performance being less than a given small probability value [1–6, 11, 12]. The mean and standard deviation are formulated as multidimensional integrals in uncertain parameters. Papers [2,4] utilized Monte Carlo (MC) for estimating statistical moments in RADO with uncertain Mach numbers. PCE has emerged as a computationally efficient alternative, used in works such as [5, 6] for RADO with uncertain Mach number and lift coefficient. Shah et al. [12] combined probabilistic and interval approaches for RADO with random and epistemic uncertainties, employing a global PCE surrogate model. Schillings et al. [11] presented a robust airfoil design using KL expansion for geometric uncertainties and PCE for quantifying output variability. Dimitrios I. [1] proposed a methodology for aerodynamic shape optimization underflow and geometric uncertainties, utilizing KL and PCE approaches for modeling and quantifying uncertainties in the drag coefficient. Unlike the KL approach used in [1, 11], Christian Sabater et al. [10] proposed a novel approach for robust optimization using quantile minimization under high-dimensional uncertainties. This approach combines Bayesian regression for quantile estimation with Bayesian optimization for improving minimum quantile determination through sequential sampling. The method is tested on robust aircraft airfoil's shock control hump design under high-dimensional geometric and operational uncertainties. Xiaosong Du and Leifur Leifsson [3] employed utility theory to formulate the objective function for aerodynamic shape optimization under uncertainty, comparing it to deterministic and standard robust design formulations in [14].

Once the mathematical expression of the robust optimization problem is defined, the efficient optimization algorithm is used to optimize the aerodynamic performance of a parameterized geometry under one or more key design point conditions. There are mainly two classes of optimization methods based on CFD simulations. The first class of optimization methods is local optimization methods, e.g., the descent method [14], which progress optimizes iteratively using the gradient of objective functions and constraints. This type of approach is widely used because of its fast convergence speed. The gradients of the aerodynamic functions, on the other hand, are complicated to calculate. In general, the adjoint equation technique has been widely used to calculate the gradient [1, 10, 11, 14].

Papers [2, 3] used the Sequential Least-Squares Programming (SLSQP) method. [1] used the Moving Asymptotes Method (MMA), which replaces the difficult nonlinear, non-convex optimization problem with a sequence of approximate convex sub-problems that are much easier to solve. The second class contains gradient-free optimization methods that use only the values of the objective function without using its derivatives, e.g., the differential evolution (DE) algorithms used in [6], and in papers [2, 4] used the particle swarm optimization (PSO) algorithms.

This paper is organized as follows. In Section 2, the FFD parametrization technique is presented. Section 3 offers the numerical methods of the CFD code and the ANN-based substitution model. Section 4 presents the mathematical formulation of a shape optimization problem under uncertainty in aerodynamics, as well as the approach used to take uncertainty into account. In Section 5, we present numerical results concerning the application of the approach of Section 4 for the aerodynamic optimization of an aircraft wing in the transonic regime. Two uncertain variables are considered in this test case: the Mach number and the angle of incidence.

2. Geometry parametric modeling

Shape parameterization has acquired a significant role in airfoil design and optimization. The parametric description of the object geometry determines the computational time cost of the optimization as well as the quality of its findings which influences the success of the optimization process.

2.1. Free-form deformation

The FFD (Free-form deformation) technique originates from the field of computer graphics [15]. It allows the deformation of an object in 2D or 3D space, regardless of the representation of that object. Instead of manipulating the object's surface directly, using the classical B-Splines or Bézier parameters of the surface, FFD techniques define a deformation field on the space embedded in a lattice built around the object. By transforming the spatial coordinates within the lattice, the FFD technique deforms the object, regardless of its geometric description.

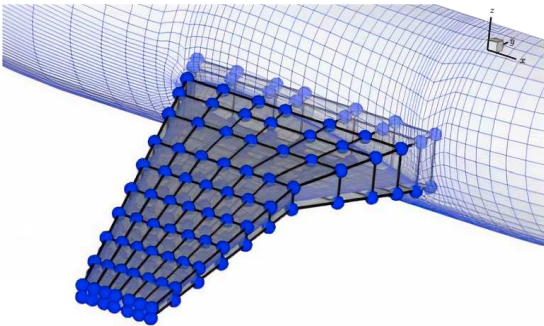


Fig. 3. Parameterization of the wing with a free-form deformation box with 84 matched nodes. The torsion is parameterized separately with 12 variables.

More precisely, we consider a three-dimensional hexahedral lattice in which the object to be deformed is integrated. Figure 3 shows an example of such a lattice built around a realistic wing. A local coordinate system (ξ, η, ζ) is defined in the lattice, with $(\xi, \eta, \zeta) \in [0, 1] \times [0, 1] \times [0, 1]$. During the deformation, the displacement Δq of each point q inside the lattice is defined here by the third order Bézier tensor product:

$$\Delta q = \sum_{i=0}^{n_i} \sum_{j=0}^{n_j} \sum_{k=0}^{n_k} B_i^{n_i}(\xi_q) B_j^{n_j}(\eta_q) B_k^{n_k}(\zeta_q) \Delta P_{ijk}, \quad (1)$$

$B_i^{n_i}$, $B_j^{n_j}$, and $B_k^{n_k}$ are the Bernstein polynomials of order n_i , n_j , and n_k .

$$B_p^n(t) = C_n^p t^p (1-t)^{n-p}, \quad (2)$$

$(\Delta P_{ijk})_{0 \leq i \leq n_i, 0 \leq j \leq n_j, 0 \leq k \leq n_k}$ are weighting coefficients, or control point displacements, which are used to monitor deformation and are considered as design variables during the shape optimization procedure.

The success of the FFD method in aerodynamic shape optimization is due to several reasons:

- The mesh topology remains fixed during the optimization, so the mesh can be regenerated automatically with high robustness (avoiding folding).
- Since the proposed technique is independent of the mesh's topology, structured and unstructured meshes can be treated similarly for configurations of complex configurations.
- The changes in the geometry are small.
- The number of parameters, which depends on the user's choice, is typically small due to order reduction techniques.

3. Analysis and surrogate modeling

The second step in assessing the aerodynamic quality of a shape is to solve the fluid mechanic's equations, which govern the behavior of the fluid around the shape. In the context of our applications, these equations are the Euler equations. In this section, we will present the numerical method used to solve these equations and the substitution model used to replace the CFD simulations.

3.1. Aerodynamic analysis

Modeling. This study is limited to three-dimensional inviscid compressible flows governed by the Euler equations, which are considered a simplification of the Navier–Stokes equations in the case of a perfect fluid, i.e., a non-viscous, non-heat conducting fluid. It comprises five conservation equations (four in 2D): a scalar equation for the mass, a vector equation for momentum, and a scalar equation for energy. The equations of state can then be written in the following conservative form:

$$\frac{\partial W}{\partial t} + \nabla \cdot \mathbf{F}(W) = 0, \quad (3)$$

where W are the conservative flow variables

$$W = \begin{pmatrix} \rho \\ \rho u \\ \rho v \\ \rho w \\ E \end{pmatrix}$$

and $\mathbf{F}(W) = (F_1(W), F_2(W), F_3(W))^T$ is the flow vector whose components are given by

$$F_1(W) = \begin{pmatrix} \rho u \\ \rho u^2 + p \\ \rho u v \\ \rho u w \\ u(E + p) \end{pmatrix}, \quad F_2(W) = \begin{pmatrix} \rho v \\ \rho u v \\ \rho w^2 + p \\ \rho v w \\ v(E + p) \end{pmatrix}, \quad F_3(W) = \begin{pmatrix} \rho w \\ \rho u w \\ \rho v w \\ \rho w^2 + p \\ w(E + p) \end{pmatrix},$$

ρ is the density, $\mathbf{U} = (u, v, w)^T$ is the velocity vector, E is the total energy per unit volume, and the pressure p verifies the law of perfect gas states:

$$p = (\gamma_p - 1) \left(E - \frac{1}{2} \rho \|\mathbf{U}\|^2 \right),$$

where γ_p is the ratio of the heat capacities at constant pressure and volume ($\gamma_p = 1.4$ for air).

Spatial discretization. The computational domain Ω is discretized by a triangulation \mathcal{T}_h , where h is the maximum edge length of \mathcal{T}_h . A discretization of Eq. (3) at the mesh node s_i is obtained by integrating (3) over the volume C_i , which is constructed around the node s_i by joining the barycenters of the tetrahedra and triangles containing s_i and the midpoints of the edges adjacent to s_i :

$$\text{Vol}_i \frac{\partial W_i}{\partial t} + \sum_{j \in N(i)} \Phi_F(W_i^n, W_j^n, \sigma_{ij}) = 0, \quad (4)$$

where W_i is the mean state of the cell and Vol_i is the volume of the cell C_i , $N(i)$ is the set of neighbouring nodes, $\Phi_F(W_i^n, W_j^n, \sigma_{ij})$ is an approximation of the integral of the flows $\mathbf{F}(W)$ on the boundary ∂C_{ij} between C_i and C_j which depends on W_i , W_j and σ_{ij} the integral of a unit normal vector on ∂C_{ij} . These numerical fluxes are evaluated using upwinding, according to the approximate Riemann solver of Roe [16].

Time integration. A first-order implicit backward scheme is employed for the pseudo-time integration of (4) to the steady state. The linearization of the numerical fluxes provides the following integration scheme:

$$\left(\frac{\text{Vol}_i}{\Delta t} + J_i^n \right) \delta W_i = - \sum_{j \in N(i)} \Phi(W_i^n, W_j^n, \sigma_{ij}), \quad (5)$$

with $\delta W_i = W_i^{n+1} - W_i^n$ and J_i^n the Jacobian matrix of the first-order numerical fluxes.

3.2. Artificial neural networks based surrogate modeling

In this study, the ANN-based surrogate model is built to replace CFD simulations during the optimization process, thus accelerating the optimization's convergence.

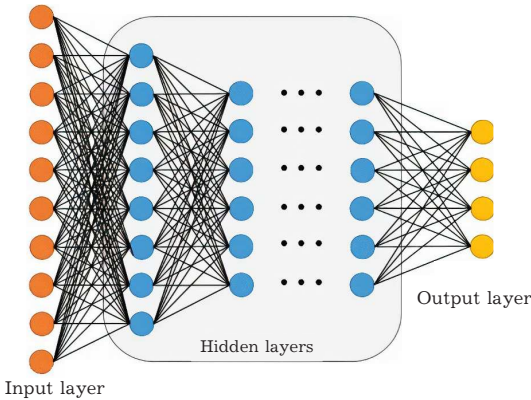
Neural networks are a type of surrogate model that can approximate a function. Neural networks propose a non-linear analytical formulation to express a function with $N_y > 1$ outputs. The functioning of biological neurons strongly inspires their design. Indeed, an artificial neuron can be seen as a transfer function allowing to transform its inputs $X = (X_1, \dots, X_{N_x}) \in \mathbf{R}^{N_x}$ into an output $Z(X) \in \mathbf{R}$ according to precise rules, depending on the use of the neuron. As their field of application is vast, this section focuses only on using neural networks for function approximation.

In this framework, a neuron is written:

$$Z(X) = \phi \left(\sum_{i=0}^{N_x} w_i X_i + b_i \right), \quad (6)$$

$w = (w_0, \dots, w_{N_x})$ are the weights for making a linear combination of the inputs, $b = (b_0, \dots, b_{N_x})$ is the bias vector, ϕ indicates the activation function in the hidden layer. Common choices of activation function are non-linear functions such as **ReLU**, **Sigmoid**, and **Tanh**. In this study we use the **Swish** function, proposed by Prajit Ramachandran et al. [17] is given by

$$\phi(x) = x(1 + e^{-x})^{-1}. \quad (7)$$



Input layer

Fig. 4. Framework of artificial neural networks.

Figure 4 shows the structure of the ANN, which consists of an input layer, hidden layers, and an output layer.

The initial step involves generating a target data set (C_D, C_L) with the assistance of the CFD model, using an input data set determined via DOE (Figure 5). These target vectors are then utilized to train the ANN model. The input layer of the ANN includes the design variables obtained through the FFD parametrization method, in addition to the Mach number M and angle of attack α . Meanwhile, the output layer of the ANN is responsible for representing the aerodynamic coefficients, specifically C_L and C_D .



Fig. 5. Data generation.

ANN's unknown weights and biases are usually randomly initialized and then iteratively adjusted to minimize the loss function (*mean squared error MSE*). Once the loss function is determined, the partial derivatives of the loss function concerning the learnable parameters ω and b can be obtained according to the chain derivation rule. The parameters will be updated via the error backpropagation algorithm and optimization algorithm *Adam* [18] based on the partial derivatives to achieve the minimum value of the loss function. This paper uses the *Tensorflow* [19] to build and train the ANN.

4. Shape optimization under uncertainty

4.1. Deterministic shape optimization problem

A shape optimization problem based on deterministic simulation minimizes a cost function \mathcal{J} , which depends on a shape Γ and state variables W . In parametric approaches, the Γ shape is represented by a small number of variables of form $\mathbf{x} = (x^i)_{i=1, \dots, n}$, which are considered optimization variables. Such a parametric approach allows replacing the initial infinite-dimensional shape optimization problem with a finite number n of unknowns. The state variables W (i.e., the physical flow fields) implicitly depend on the shape variables through the state equations $\mathcal{R}(\mathbf{x}, W(\mathbf{x}, \mathbf{a})) = 0$ (\mathcal{R} are the Euler equations (3)

in this study), where $\mathbf{a} = (a^j)_{j=1,\dots,m}$ represents some parameters that define the operating conditions such as the Mach number, the angle of attack, etc. Finally, a general parametric form optimization problem can be expressed as follows:

$$\begin{cases} \text{Minimize } \mathcal{J}(\mathbf{x}, W(\mathbf{x}, \mathbf{a})), \\ \mathbf{x} \in \mathbf{R}^n \\ \text{Subject to } \mathcal{C}(\mathbf{x}, W(\mathbf{x}, \mathbf{a})) \leq 0, \end{cases} \quad (8)$$

where \mathcal{C} represents additional constraints (physical or geometric).

An optimal shape generally does not consider the uncertainty or variability of certain parameters or data that will affect the performance of the shape in a real situation. Therefore, it is important to achieve stability of the solution, as a deterministic optimization approach (single-point method) could tend towards an “over-optimization” problem (Figure 6), giving high performance in correspondence with the shape point, but giving poor off-design characteristics.

Referring to Figure 6, the function has an absolute extreme and a relative extreme corresponding to the value x_1 and x_2 of the parameter x . In this case, the operational uncertainties could be represented by the tolerance $2 \times \Delta x$ of the input parameter x . A deterministic optimization, which does not consider fluctuations, will detect the point x_1 . On the contrary, the robust optimization will detect the point x_2 , which corresponds to the highest value of stability of the function in the tolerance range x .

We now mention robust shape methods that consider fluctuating (uncertain) parameters.

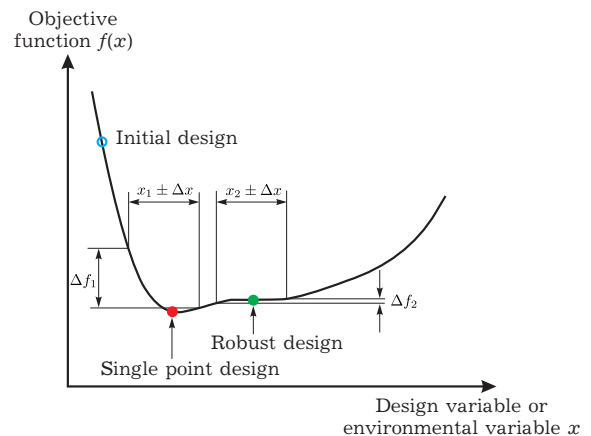


Fig. 6. Robust design and single-point design [4].

4.2. Robustness methods

Deb and Gupta [20] extended an existing approach that finds robust solutions for single-objective optimization problems to multi-objective with dynamic parameters. They defined the average effective objective functions instead of the original objective functions.

Consider a general optimization problem of the following type:

$$\begin{aligned} &\text{Minimize } \mathcal{J}(\mathbf{x}), \\ &\text{Subject to } \mathbf{x} \in \mathcal{S}, \end{aligned} \quad (9)$$

where \mathcal{S} is the feasible search space.

To avoid obtaining the global optimal solutions which are very sensitive to such a variable perturbation in their neighborhood, the following two approaches are defined for robust optimization by Deb and Gupta [20].

Definition 1 (Robust solution of type I). For the minimization of an objective function $\mathcal{J}(\mathbf{x})$, a solution \mathbf{x}^* is called a robust solution of type I, if it is the global minimum of the mean effective function $\mathcal{J}^{\text{eff}}(\mathbf{x})$ defined with respect to a δ -neighborhood as follows:

$$\begin{aligned} &\text{Minimize } \mathcal{J}^{\text{eff}}(\mathbf{x}) = \frac{1}{|\mathcal{B}_\delta(\mathbf{x})|} \int_{\mathbf{y} \in \mathcal{B}_\delta(\mathbf{x})} \mathcal{J}(\mathbf{y}) d\mathbf{y}, \\ &\text{Subject to } \mathbf{x} \in \mathcal{S}, \end{aligned} \quad (10)$$

where $\mathcal{B}_\delta(\mathbf{x})$ is the δ -neighborhood of the solution \mathbf{x} and $|\mathcal{B}_\delta(\mathbf{x})|$ is the hypervolume of the neighborhood.

In this method, a mean function measure (\mathcal{J}^{eff}) is optimized instead of the objective function(s). To use it in practice, robust optimization starts by creating a set of random candidate solutions for a particular problem. Each candidate solution is evaluated by the average of the H solutions generated around it. The solutions are chosen randomly (or in a structured way, such as the Latin hypercube method) from the hypervolume ($\mathcal{B}_\delta(\mathbf{x})$) of radius δ around the solutions. Where δ denotes the maximum possible level of perturbation.

Deb and Gupta [20] proposed a new and more practical approach that allows a user to define the desired degree of robustness in a problem. This approach consists of calculating the normalized difference in values between the value of the effective mean function (\mathcal{J}^{eff}) and the original function \mathcal{J} itself and declaring a solution to be robust if the normalized difference is below a chosen threshold (δ).

Definition 2 (Robust solution of type II). For the minimization of an objective function $\mathcal{J}(\mathbf{x})$, a solution \mathbf{x}^* is called a robust solution of type II, if it is the global minimum of the mean effective function $\mathcal{J}^{\text{eff}}(\mathbf{x})$ defined with respect to a δ -neighborhood as follows:

$$\begin{aligned} & \text{Minimize } \mathcal{J}(\mathbf{x}), \\ & \text{Subject to } \frac{\|\mathcal{J}^{\text{eff}}(\mathbf{x}) - \mathcal{J}(\mathbf{x})\|}{\|\mathcal{J}(\mathbf{x})\|} \leq \eta, \\ & \mathbf{x} \in \mathcal{S}, \end{aligned}$$

with $\delta \in [0, 1]$. The operator $\|\cdot\|$ can be any suitable norm measure.

5. Robust aerodynamic optimization of an aircraft wing

5.1. Description of the problem

The test case corresponds to the shape optimization of a realistic 3D aircraft wing for a transonic regime (Euler equations (3)). The nominal operating conditions are defined by the free-flow Mach number $M_\infty = 0.83$ and the incidence $\alpha = 2$. The initial shape of the wing is shown in Figures 7.

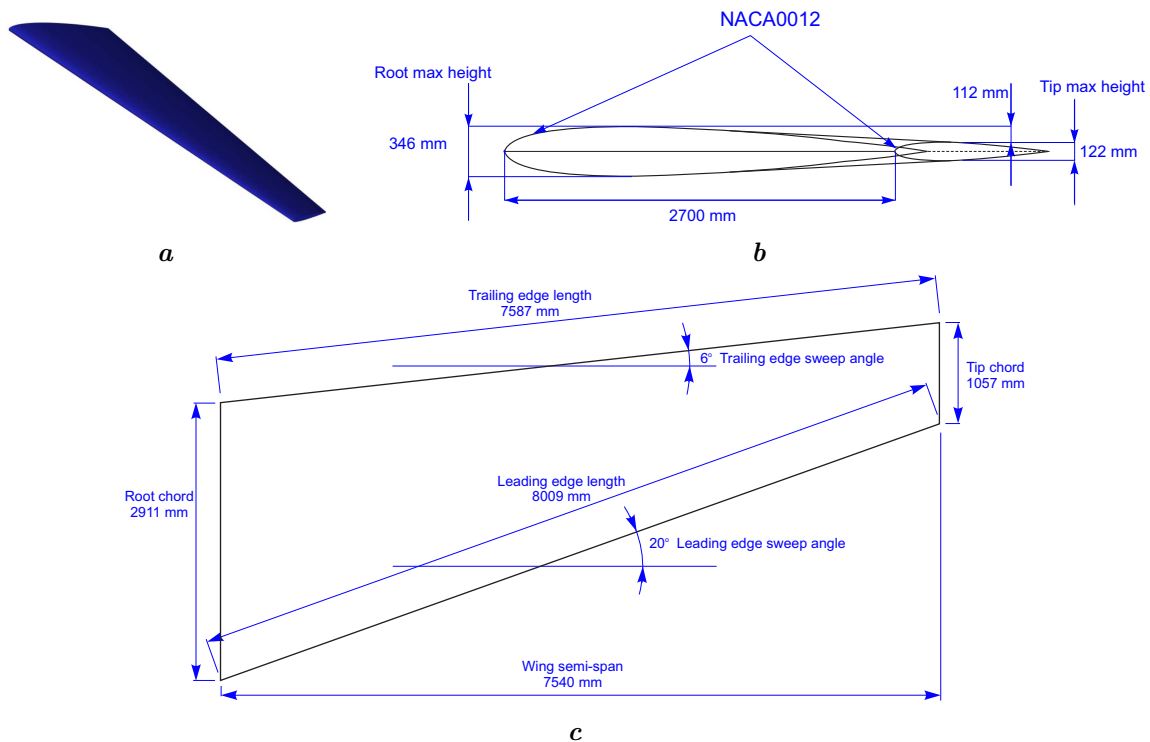


Fig. 7. The initial shape of the wing.

In this case study, we use the FFD technique described in section 2.1, where a box surrounding the wing was defined to reduce its dimensions without cutting the wing surface. Then, the dimensional space was explored by considering 12 control point variables x , the shape variables defined for the optimization problem.

Twelve parameters (x_i) represent the displacement of the control points of the FFD parametrization:

- A lattice is built around the initial shape of the wing with a margin of (1500, 3000, 0) on the (X, Y, Z) axes respectively, following the shape of the wing along the Z axis.

- The margin (1500, 3000, 0) allows a part of the CFD mesh to be included in addition to the wing in the deformation zone.
- The lattice is of order (3, 1, 4). The total number of control points is thus $4 \times 2 \times 5 = 40$.
- Only the inner points are movable and only in the Y direction, the aim being to optimize the airfoil. This reduces the freedom of the lattice to twelve degrees of freedom.
- Thus the number of parameters of the shape by this FFD parametrization process is 12 (see Figure 8).
- As mentioned, the deformation includes a part of the CFD mesh in addition to the wing (see Figure 8). To ensure good mesh quality the displacement of the control points is therefore restricted to the interval $[-200, 200]$ ¹². The design space is therefore $[-200, 200]$ ¹².

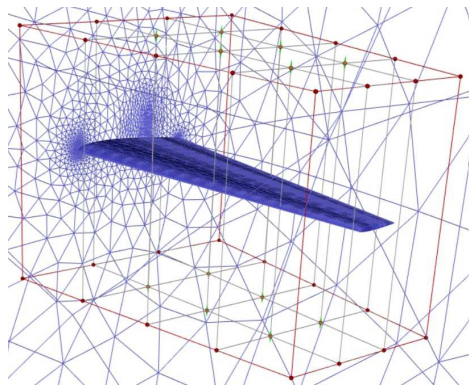


Fig. 8. Parametrization by FFD and meshing.

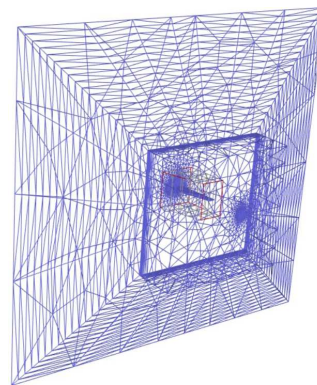


Fig. 9. Unstructured mesh.

Spatial discretization. Our solver uses an unstructured mesh of 31124 nodes and 173445 tetrahedral elements generated around the wing, including a refined area near the shock (see Figure 9). The flow is simulated by solving the compressible Euler equations (3) with a finite volume method. As far as the flow domain Ω is discretized by tetrahedriations.

Surrogate model. The Surrogate model is a neural network with **Swich** as the activation function and considering the **Adam** optimization algorithm. The model was trained by 1000 samples generated using the quasi-stochastic LHS (Latin Hypercube Sampling) method. Each sample contains 12 parametrization variables, which vary in $[-200, 200]$. In addition to Mach number M which varies in $[0.83 \pm 0.04]$ and incidence α which varies in $[2 \pm 0.04]$. For each point, an analysis was performed to evaluate the aerodynamic coefficient, drag C_D and lift C_L . A neural network with three hidden layers containing 18 neurons was trained to predict C_D and C_L . Eighty percent is used to train the model and 20% for validation. Figure 10 shows the error evaluation as a function of the number of epochs (training curve). Figure 11 represents the effective values of the objective function evaluated by the high-fidelity model at the predicted optima and shows the relative errors.

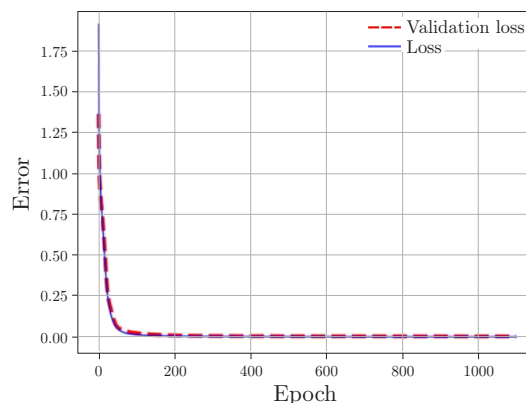


Fig. 10. Learning curve.

5.2. Test case 1

The problem of optimizing the shape of an aerofoil is usually formulated in terms of reducing drag under the constraints of maximum lift. Drag and lift are generally represented by their corresponding coefficients C_D and C_L . Typically, the set of variables used to optimize the airfoil performance corresponding to the Mach number M , the incidence α , and the control variables are the 12 FFD parameters defined on $[-200, 200]$. Thus we define the objective function as the drag-to-lift ratio of a

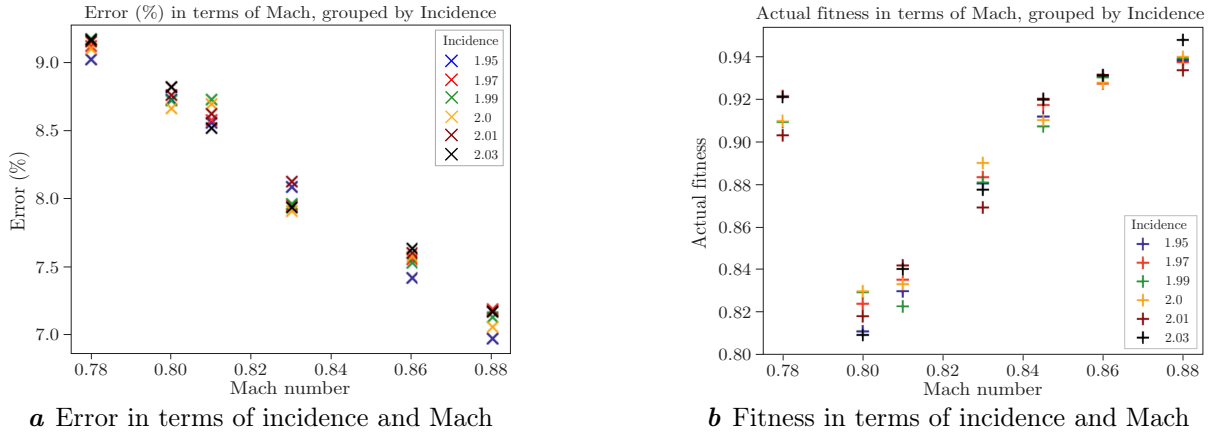


Fig. 11. Error and fitness in terms of incidence and Mach.

profile (Drag-To-Lift-Ratio), the function of problem (11). The optimization problem is formulated as follows:

$$\begin{aligned} \text{Minimize } \mathcal{J}(\mathbf{x}, M, \alpha) &= \frac{C_D(\theta)/C_{D_0}(\theta)}{C_{L_0}(\theta)/C_{L_0}(\theta)}, \\ \text{Subject to } \mathbf{x} &\in [-200, 200]^{12}, \end{aligned} \tag{11}$$

where C_{D_0} and C_{L_0} are respectively the drag and lift of the initial configuration and $\theta = (\mathbf{x}, M, \alpha)$.

5.2.1. Deterministic optimization

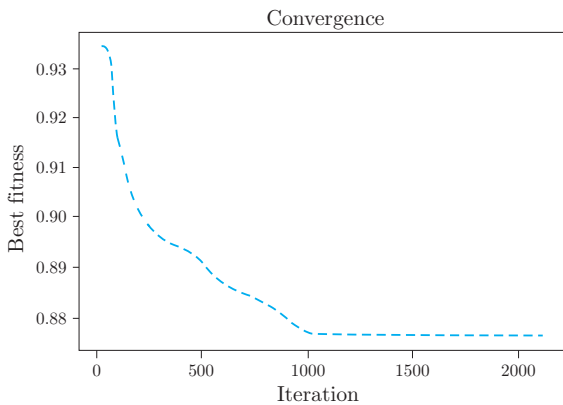
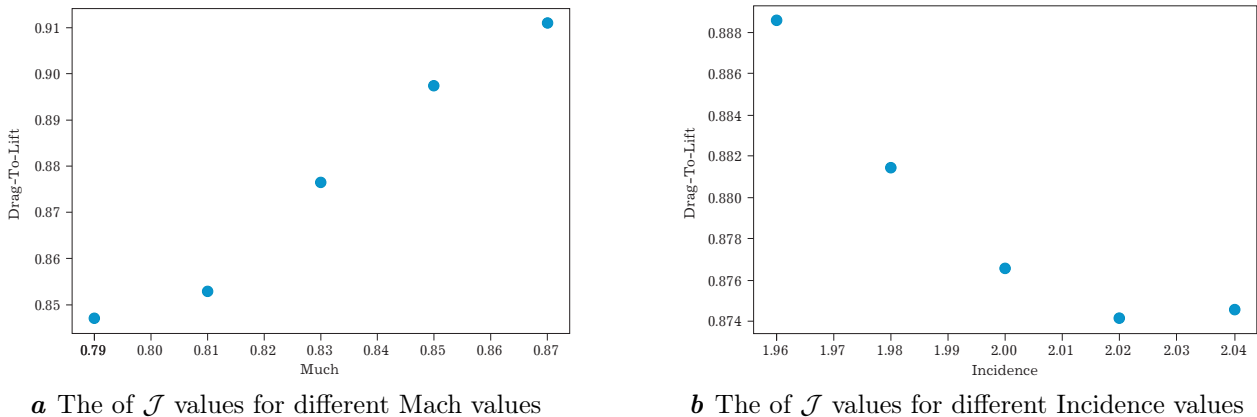


Fig. 12. Convergence curve of the PSO algorithm.

We first solve the deterministic optimization problem (12), with fixed operating conditions. Thus, the Mach number is assumed to have its nominal value $M_\infty = 0.83$, and the incidence has the value $\alpha = 2^\circ$. The convergence curve of the PSO algorithm is shown in Figure 12. As can be seen from the figure, the PSO algorithm obtains the optimal result at the 1000th iteration.

We now analyze the variation of the values of the Drag-To-Lift-Ratio function of problem (11) for the optimal shape found when the Mach number and the Incidence vary around its nominal values. Figure 13a compares the values of the Drag-to-Lift-Ratio function for different Mach numbers and fixed Incidence equal 2° . Figure 13b compares the Drag-To-Lift-Ratio values for different Incidence values, and the fixed Mach number equals 0.83.



a The of \mathcal{J} values for different Mach values

b The of \mathcal{J} values for different Incidence values

Fig. 13. Variation of the Drag-To-Lift-Ratio function as a function of incidence and mach number for the optimal shape.

As can be seen from Figure 13a, the Drag-To-Lift-Ratio function increases sharply when the Mach number exceeds its nominal value. Similarly, it can be observed from Figure 13b that the Drag-To-Lift-Ratio function decreases significantly when the incidence value is lower than its nominal value.

5.2.2. Robust optimization

In this section, we study the propagation of uncertainty. We distinguish three cases, first, we consider the uncertainty relative to the Mach number M around the nominal value 0.38 and the variable Incidence fixed equal to the nominal value 2. In the second case, the Mach number M is fixed at the nominal value 0.38, and the incidence variable α is considered uncertain. In the last case. Both the Mach number M and the incidence α are considered uncertain variables.

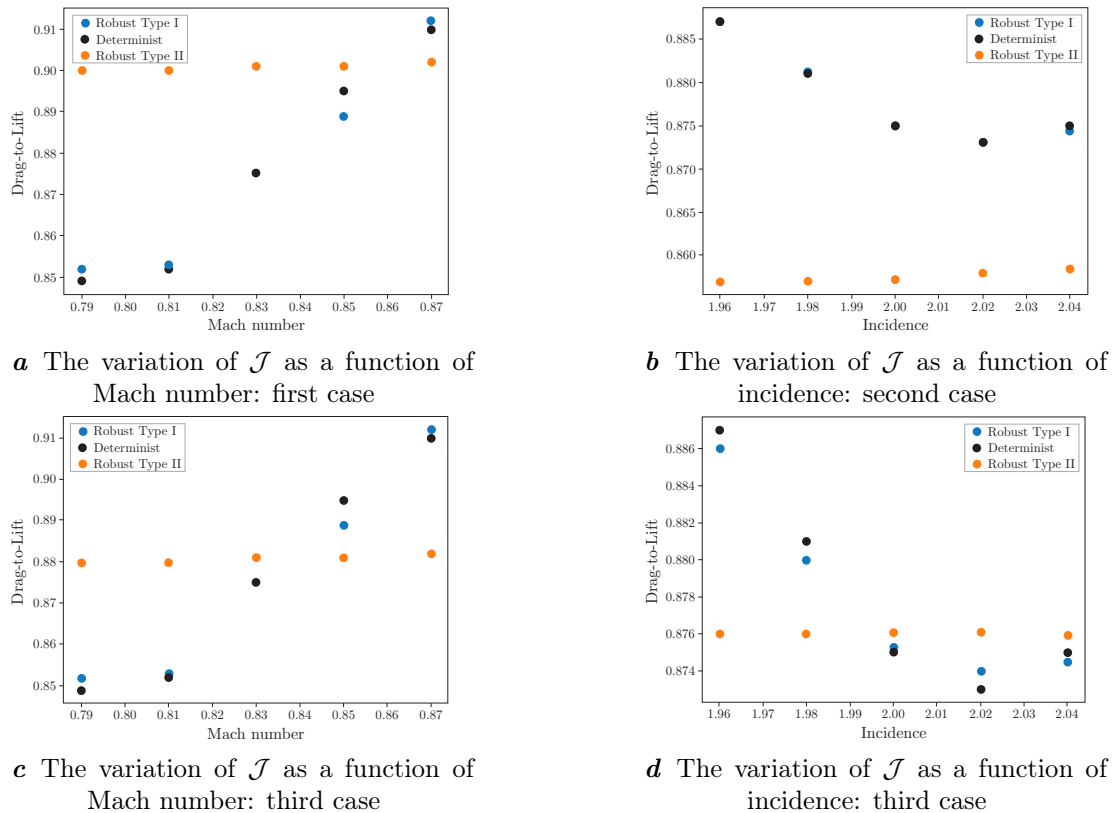


Fig. 14. The variation of the Drag-To-Lift-Ratio function as a function of Mach number and incidence for robust type I, II, and optimal shapes.

In the robust type I method, the effective objective function \mathcal{J}^{eff} is optimized, with each solution evaluated on a ball of radius $\delta = 0.04$ by averaging $h = 100$ points generated using the Latin hypercube strategy. On the other hand, for the robust type II approach, the \mathcal{J} function is optimized at the nominal point, with a constraint used to confirm the robustness of the solution. The PSO algorithm is employed to solve both type I and type II problems with $\eta = 0.1$.

In Figure 14, the values of the Drag-To-Lift-Ratio function are plotted for various Mach and incidence values, representing the robust type I and II forms as well as the optimal form (blue, orange, and green). It can be observed that the robust type I solution and the deterministic solution exhibit some similarities. However, the robust type II solution demonstrates perfect stability, highlighting its robustness. Although the robust solution may be suboptimal at certain design points compared to the deterministic optimal solution, as depicted in Figure 14d, it offers greater stability in dealing with off-design variations.

In Figure 15, we illustrate the isobaric pressure lines on the wing surfaces for the initial shape and the robust type II shapes in three cases. It is evident that the optimization process has effectively reduced the presence of shock waves. Indeed, the flow appears smoother in Figures 15b, 15c, and 15d when compared to the initial shape 15a, where higher pressure gradients are observed.

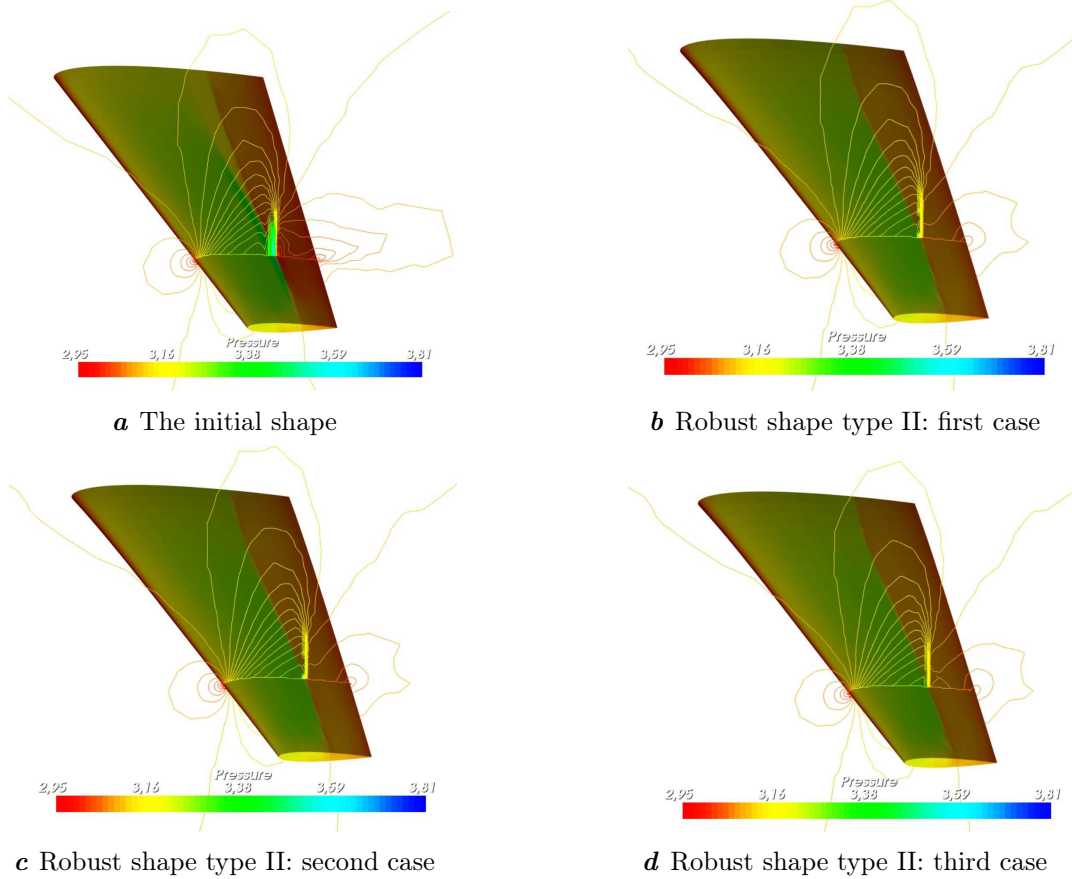


Fig. 15. Pressure fields and isobars on the surface of the robust shapes type II and the initial shape.

5.3. Test case 2

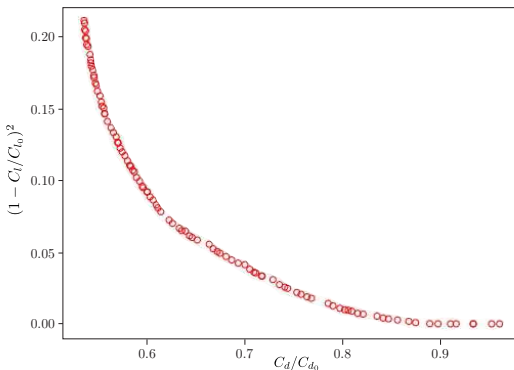


Fig. 16. The Pareto optimal solution.

algorithm solves the problem with a population of 100 individuals over 200 generations. The Pareto front obtained is represented in Figure 16.

Robust optimization. The robust type I solution is obtained by solving the problem using the NSGA2 algorithm with a population of 100 individuals over 200 generations. The resulting Pareto front is shown in Figure 17a. On the other hand, for the robust type II solution, we use the same NSGA2 algorithm with a population of 100 individuals over 200 generations, with $\eta = 0.8$. The resulting Pareto front is shown in Figure 17.

Comparison between the robust Deb solutions and the deterministic solutions. As soon as we obtain the optimal solutions illustrated by two Figures 17, we compute the values of C_d/C_{d_0} and $(1 - C_l/C_{l_0})^2$ evaluated in these solutions. As a result, the graph of the Pareto edges given in Figure 18 is drawn.

In this test case, we consider two objective functions, $\mathcal{J}_1 = \frac{C_D(\theta)}{C_{D_0}(\theta)}$ and $\mathcal{J}_2 = \left(1 - \frac{C_L(\theta)}{C_{L_0}(\theta)}\right)^2$. The drag will be reduced when minimizing \mathcal{J}_1 automatically. On the other hand, minimizing \mathcal{J}_2 means maximizing the lift. Therefore, the goal of aerodynamic profile optimization is achieved,

$$\text{Minimize } \mathcal{J}(\mathbf{x}, M, \alpha) = \left(\frac{C_D(\theta)}{C_{D_0}(\theta)}, \left(1 - \frac{C_L(\theta)}{C_{L_0}(\theta)}\right)^2 \right), \quad (12)$$

Subject to $\mathbf{x} \in [-200, 200]^{12}$.

We first solve the deterministic optimization problem (12), with fixed operating conditions. Thus, the Mach number is assumed to have its nominal value $M_\infty = 0.83$, and the incidence has the value $\alpha = 2^\circ$. The NSGA-II

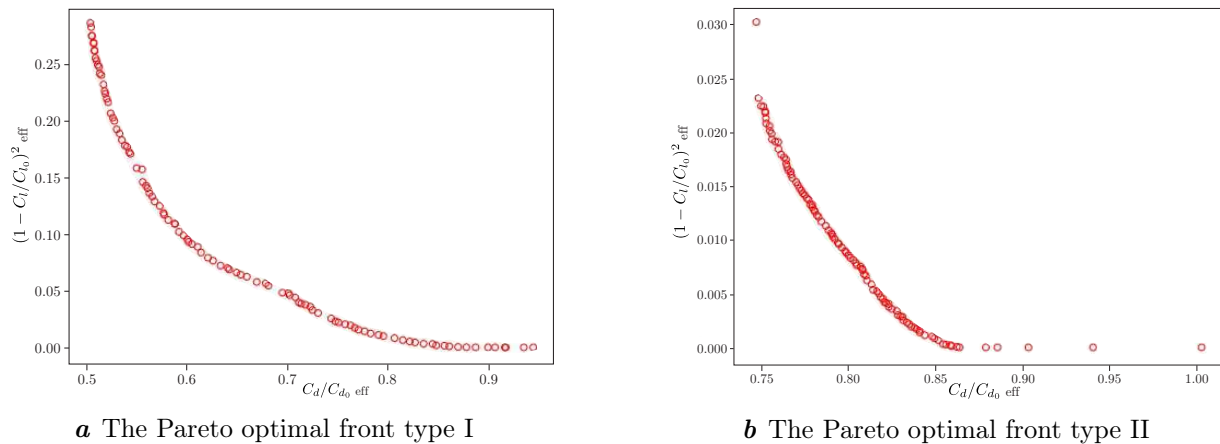


Fig. 17. Pareto robust fronts.

By examining the Pareto fronts of Figure 18, we notice that the approach of Deb more particularly the approach type II reduced the solutions. And this is consistent with the result of Deb [20].

6. Conclusion

In this study, we addressed the problem of aerodynamic shape optimization with uncertain operating conditions. We based our approach on two robust optimization methods proposed by Deb, which utilize different procedures (type I and II). These proposed approaches were applied to the robust aerodynamic design optimization of transonic wings, with uncertain Mach number and angle of attack in two test cases.

The FFD method was used to parameterize the wing control profiles, and an ANN model was established with design variables as inputs and aerodynamic parameters as outputs. The ANN-based surrogate model was trained using the Adam algorithm and validated by predicting lift and drag coefficients of aerodynamic profiles in a test group, with results indicating that the ANN-based surrogate model can provide more accurate predictions.

We integrated Deb's type I and II approaches into the deterministic PSO and NSGA-II algorithms to improve the convergence rate and global search capability. These new algorithms are R-PSO and R-NSGA-II, with "R" indicating robustness. The robust optimizations of the transonic wing were performed using the R-PSO and R-NSGA-II frameworks with the ANN-based surrogate model. Our study found that the used approaches are quite effective in considering uncertainties in an automated shape optimization procedure.

Acknowledgments

The entire authors of this research are utterly grateful to the Arab Fund for Economic and Social Development (AFESD) for financial support for this work.

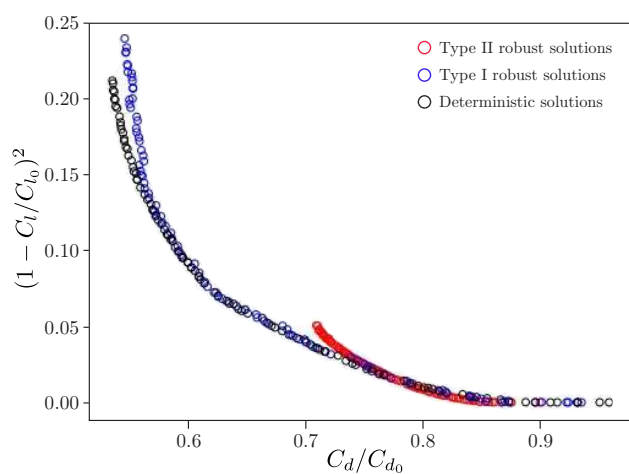


Fig. 18. The Pareto fronts.

[1] Papadimitriou D. I., Papadimitriou C. Aerodynamic shape optimization for minimum robust drag and lift reliability constraint. *Aerospace Science and Technology*. **55**, 24–33 (2016).

- [2] Nagawkar J., Leifsson L. Applications of polynomial chaos-based cokriging to simulation-based analysis and design under uncertainty. *ASME 2020 International Design Engineering Technical Conferences and Computers and Information in Engineering Conference, IDETC-CIE 2020*. **11B-2020**, V11BT11A046 (2020).
- [3] Du X., Leifsson L. Optimum aerodynamic shape design under uncertainty by utility theory and metamodelling. *Aerospace Science and Technology*. **95**, 105464 (2019).
- [4] Tao J., Sun G., Guo L., Wang X. Application of a PCA-DBN-based surrogate model to robust aerodynamic design optimization. *Chinese Journal of Aeronautics*. **33** (6), 1573–1588 (2020).
- [5] Zhao H., Gao Z., Gao Y., Wang C. Effective robust design of high lift NLF airfoil under multi-parameter uncertainty. *Aerospace Science and Technology*. **68**, 530–542 (2017).
- [6] Wu X., Zhang W., Song S. Robust aerodynamic shape design based on an adaptive stochastic optimization framework. *Structural and Multidisciplinary Optimization*. **57** (3), 639–651 (2018).
- [7] Sabater C., Bekemeyer P., Görtz S. Efficient Bilevel Surrogate Approach for Optimization Under Uncertainty of Shock Control Bumps. *AIAA Journal*. **58** (12), 5228–5242 (2020).
- [8] Abou El Majd B. Parameterization adaption for 3D shape optimization in aerodynamics. *International Journal of Science and Engineering*. **6** (1), 61–69 (2014).
- [9] Désidéri J.-A., Abou El Majd B., Janka A. Nested and selfadaptive Bézier parameterizations for shape optimization. *Journal of Computational Physics*. **224** (1), 117–131 (2007).
- [10] Sabater C., Le Maître O., Congedo P. M., Görtz S. A Bayesian approach for quantile optimization problems with high-dimensional uncertainty sources. *Computer Methods in Applied Mechanics and Engineering*. **376**, 113632 (2021).
- [11] Schillings C., Schmidt S., Schulz V. Efficient shape optimization for certain and uncertain aerodynamic. *Computers & Fluids*. **46** (1), 78–87 (2011).
- [12] Shah H., Hosder S., Koziel S., Tesfahunegn Y. A., Leifsson L. Multi-fidelity robust aerodynamic design optimization under mixed uncertainty. *Aerospace Science and Technology*. **45**, 17–29 (2015).
- [13] Moussaoui Z., El Bakkali H., Karafi Y., Abou El Majd B. Bayesian Approach for Aerodynamic Shape Robust Optimization. *IISE Annual Conference and Expo 2023*. 2231 (2023).
- [14] Mazaheri K., Nejati A. The Multi-point Optimization of Shock Control Bump with Constant-Lift Constraint Enhanced with Suction and Blowing for a Supercritical Airfoil. *Flow, Turbulence and Combustion*. **96** (3), 639–666 (2016).
- [15] Sederberg T., Parry S. Free-Form Deformation of Solid Geometric Models. *ACM SIGGRAPH Computer Graphics*. **20** (4), 151–160 (1986).
- [16] Roe P. L. Approximate Riemann solvers, parameter vectors, and differences scheme. *Journal of Computational Physics*. **43** (2), 357–371 (1981).
- [17] Ramachandran P., Zoph B., Le Q. V. Searching for activation functions. Preprint arXiv:1710.05941 (2017).
- [18] Kingma D. P., Ba J. L. Adam: A method for stochastic optimization. Preprint arXiv:1412.6980 (2014).
- [19] Abadi M., Barham P., Chen J., Chen Z., Davis A., Dean J., Devin M., Ghemawat S., Irving G., Isard M., Kudlur M., Levenberg J., Monga R., Moore S., Murray D. G., Steiner B., Tucker P., Vasudevan V., Warden P., Wicke M., Yu Y., Zheng X. Tensorflow: A system for large-scale machine learning. *12th USENIX Symposium on Operating Systems Design and Implementation (OSDI 16)*. 265–283 (2016).
- [20] Deb K., Gupta H. Introducing robustness in multi-objective optimization. *KanGAL Report 2004–2016*, Kanpur Genetic Algorithms Laboratory, Indian Institute of Technology, Kanpur, India (2004).

Надійна оптимізація форми за допомогою сурогатного моделювання крила літака на основі штучних нейронних мереж

Муссауї З.¹, Карафі Ю.¹, Абу Ель Маджд Б.^{1,2}

¹Лабораторія LMSA, факультет природничих наук, Університет Мохаммеда V у Рабаті, Марокко

²Університет Лілля, 59655 Вільньов-д'Аск, Франція

Оптимізація аеродинамічної форми є дуже активною областю досліджень, яка стикається з надзвичайно складними задачами обчислювальної гідродинаміки (CFD), оптимізації з диференціальними рівняннями у частинних похідних (PDE) як обмеженнями та відповідним обробленням невизначеностей. Це включає в себе розробку надійних методологій проектування, які є обчислювально ефективними, зберігаючи бажаний рівень точності в процесі оптимізації. У статті розглядаються проблеми оптимізації аеродинамічної форми, пов'язані з невизначеними умовами експлуатації. Після огляду можливих підходів до врахування невизначеностей модель штучної нейронної мережі (ANN) використовується для апроксимації аеродинамічних коефіцієнтів при зміні умов експлуатації. Використовуються надійні підходи до вирішення задач надійної оптимізації на основі детермінованих вимірювань, натхненні роботою Деба [Deb K., Gupta N. Introducing robustness in multi-objective optimization. KanGAL Report 2004–2016, Kanpur Genetic Algorithms Laboratory, Indian Institute of Technology, Kanpur, India (2004)]. Перша процедура є прямим розширенням методики, що використовується для одноцільової оптимізації. Другий — більш практичний підхід, що дозволяє користувачеві визначити бажаний ступінь надійності проблеми. Ці підходи були перевірені та підтвержені у випадку оптимізації профілю крила літака в трансзвуковому режимі з урахуванням двох невизначених змінних: числа Маха та кута падіння.

Ключові слова: *оптимізація форми; аеродинамічний аналіз; деформація вільної форми; сурогатна модель; моделювання невизначеності; штучні нейронні мережі.*